Supporting Information

In-Plane Anisotropy in the Layered Topological Insulator $Ta_2Ni_3Te_5$ Investigated via TEM and Polarized Raman Spectroscopy

Kamal Harrison[1], Dylan A. Jeff[1], Jonathan M. DeStefano[2], Olivia Peek[2], Akihiro Kushima[3], Jiun-Haw Chu[2], Humberto R. Gutiérrez[,4], Saiful I. Khondaker*[,1,5]*

[1]NanoScience Technology Center, and Department of Physics, University of Central Florida, Orlando, FL 32816, USA

[2]Department of Physics, University of Washington, Seattle, WA 98195, USA

[3]Department of Materials Science and Engineering, and Advanced Materials Processing and Analysis Center, University of Central Florida, Orlando, FL, USA

[4]Department of Physics, University of South Florida, Tampa, FL, 33620, USA

[5]School of Electrical Engineering and Computer Science, University of Central Florida, Orlando, FL 32826, USA

*Corresponding Authors: saiful@ucf.edu, humberto3@usf.edu

S1. Scotch Tape Exfoliations of $Ta_2Ni_3Te_5$

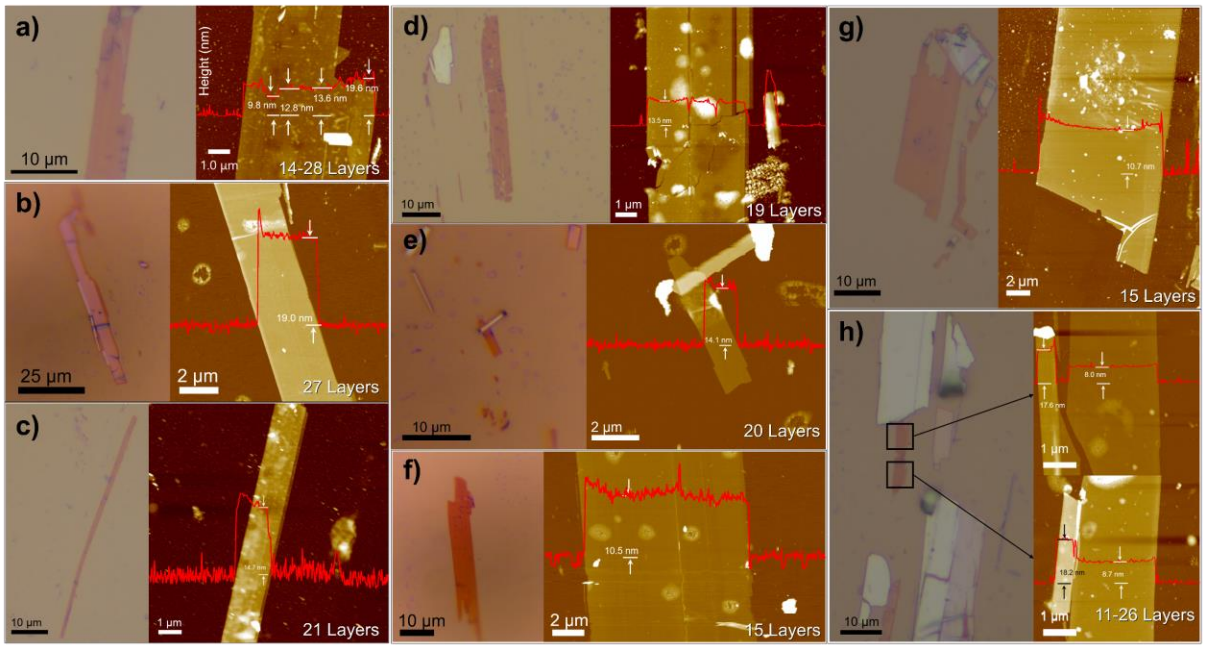

Supporting Figure S1. Results of all scotch tape exfoliations on $Ta_2Ni_3Te_5$, using the scotch tape approach, from 28 to 11 layers. For each flake, an optical micrograph is displayed on the left and the corresponding atomic force micrograph is displayed on the right with the height of the flake outlined. The number of layers was determined based on the overall heights of each flake divided by the interatomic spacing (0.6955 nm) calculated via XRD. (a) displays additional height values on the same flake of figure 1e in the main text.

S2. SEM Images of Samples Exfoliated via Sonication

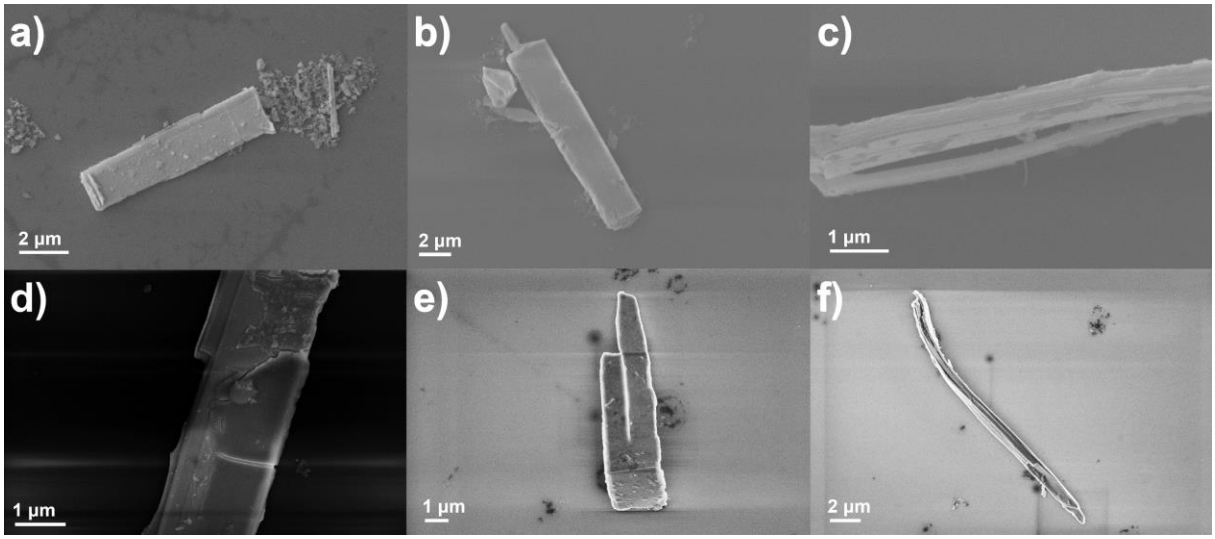

Supporting Figure S2. Scanning electron microscopy (SEM) images of $Ta_2Ni_3Te_5$ exfoliated via sonication of a crystal in an isopropanol solution and subsequently deposited on SiO_2 substrate. These flakes come in a variety of sizes, including a few-micron flake (a) and the 18 µm long flake (b).

S3. Fourier Transform of TEM Images

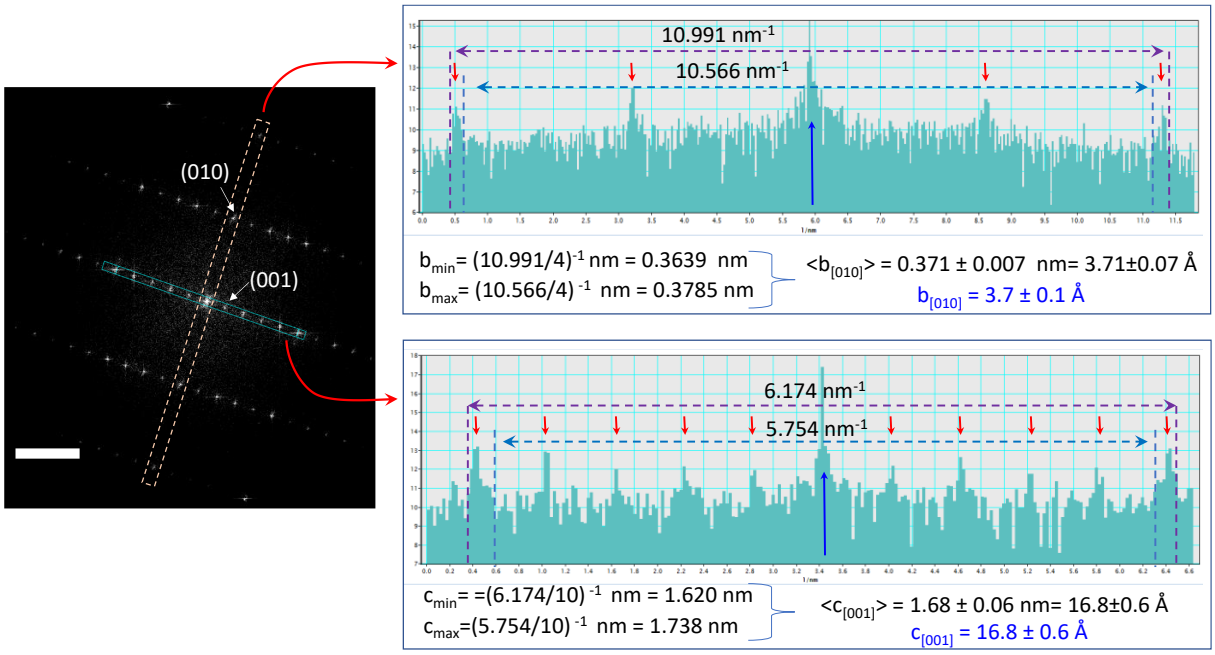

Supporting Figure S3. Calculation of the in-plane lattice parameters using the FT pattern from figure 2b in the main text. In the left panel, highlighted by the dashed long boxes, we extract the intensity profiles along the two directions in the reciprocal space that contain the spots corresponding to crystal directions parallel to the [010] and [001], respectively. Subsequently (in the right panels) we measure the distance (in reciprocal space) between the outer most peaks in the profile and divide it by the number of peaks in between. The red arrows indicated these peaks, including the FT central spot highlighted with the blue arrow. The inverse of this distance gives the value of the lattice parameter along these crystal directions. Given that all peaks have certain width, which contributes to the error in the calculation, we measured the maximum and the minimum distance taking as reference the edges of the peaks (see the right panels) and calculated the lattice parameter for each case, then the average of those two values was reported

as the interplanar distance in each direction. For each direction, the uncertainty of the measurement was calculated as the differences between the average value and the maximum and minimum. We used the largest calculated uncertainty (± 0.6Å) to report both values ($b_{[010]}$ and $c_{[001]}$) in the main text.

S4. TEM Analysis, Simulation, and Diffraction

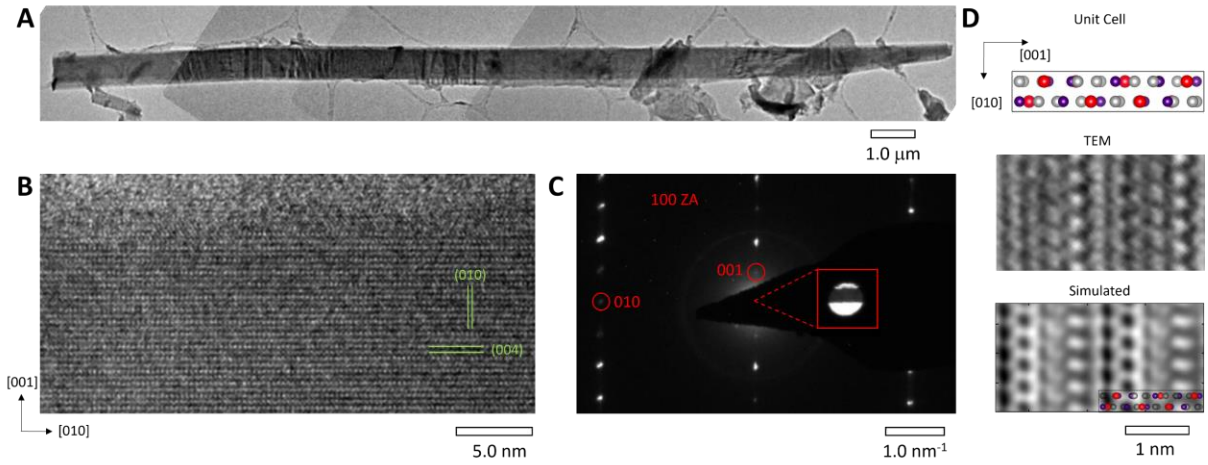

Supporting Figure S4. Electron diffraction and HRTEM image simulation including (a) low magnification image of the flake used to compare simulations, (b) additional HRTEM of the flake, (c) the diffraction pattern of the flake with an inset of the central spot defocused to correlated the image orientation (in the real space) with the diffraction pattern (reciprocal space), and (d) a comparison of the simulated result with the HRTEM image (taken from figure 2c) and the predicted unit cell of the material. The image simulations were done using 300 kV acceleration voltage, -80 nm defocus, and 30 nm thickness in [100] as input parameters.

S5. Electron Diffraction Pattern of Additional Samples

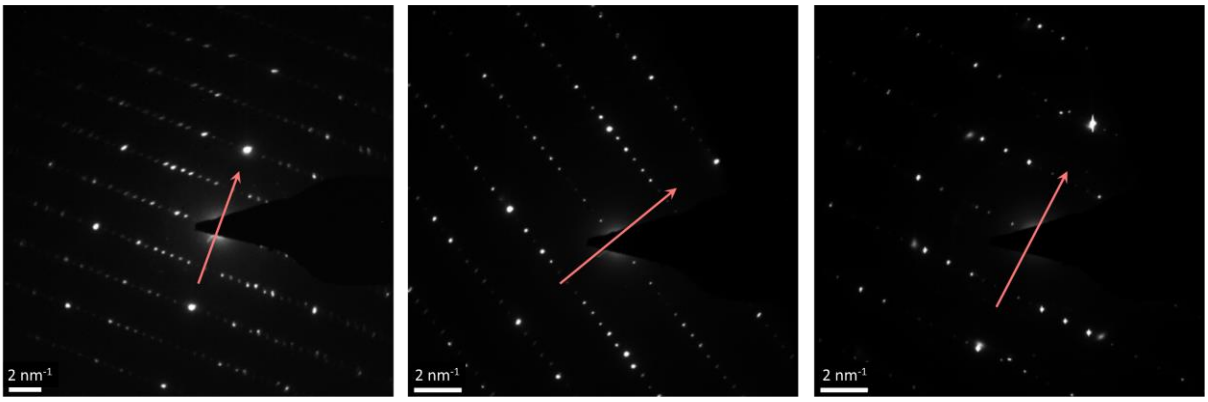

Supporting Figure S5. Electron diffraction patterns of three more strips. The red arrows indicate the direction of the long axis of the strips. These patterns were used to confirm the b and c lattice constants.

S6. Predicted Raman Fitting Corresponding to Figure 5

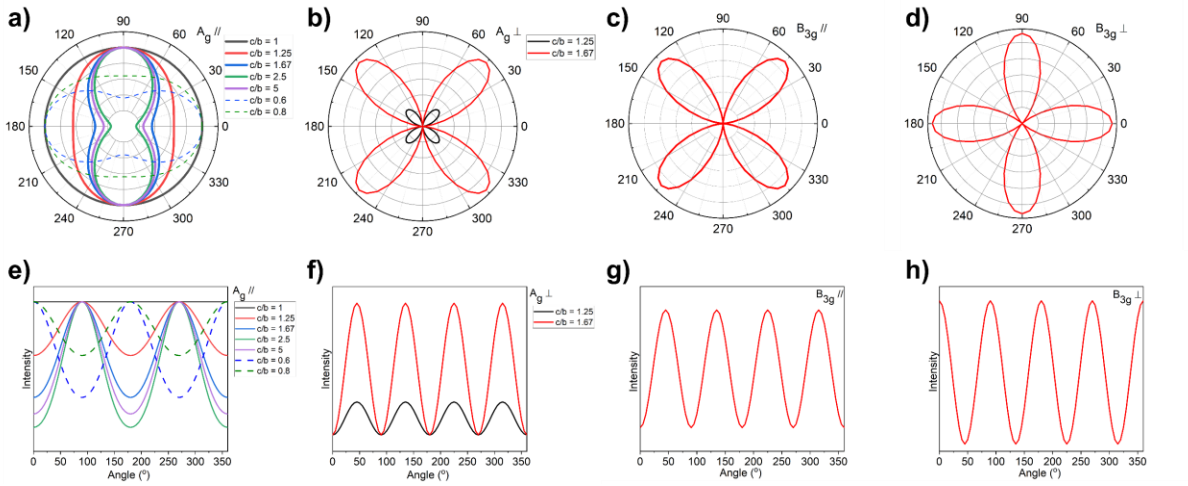

Supporting Figure S6. Polar and cartesian plots for the (a,e) $A_g^{\parallel}$, (b,f) $A_g^{\perp}$, (c,g) $B_{3g}^{\parallel}$, and (d,h) $B_{3g}^{\perp}$ modes according to equations 2-5 using real Raman tensor elements. Note that the A_g curves for different values of c/b are distinct and follow the experimental data for some peaks, as stated in the main text, but few peaks (see Supporting Figure S4) do not fit well using only real tensor components. We also note that the B_{3g} modes are predicted to have four-fold symmetry, which clearly match the experimental data for the Raman peak at 63cm^{-1}.

S7. Raman Fitting for Parallel Configuration

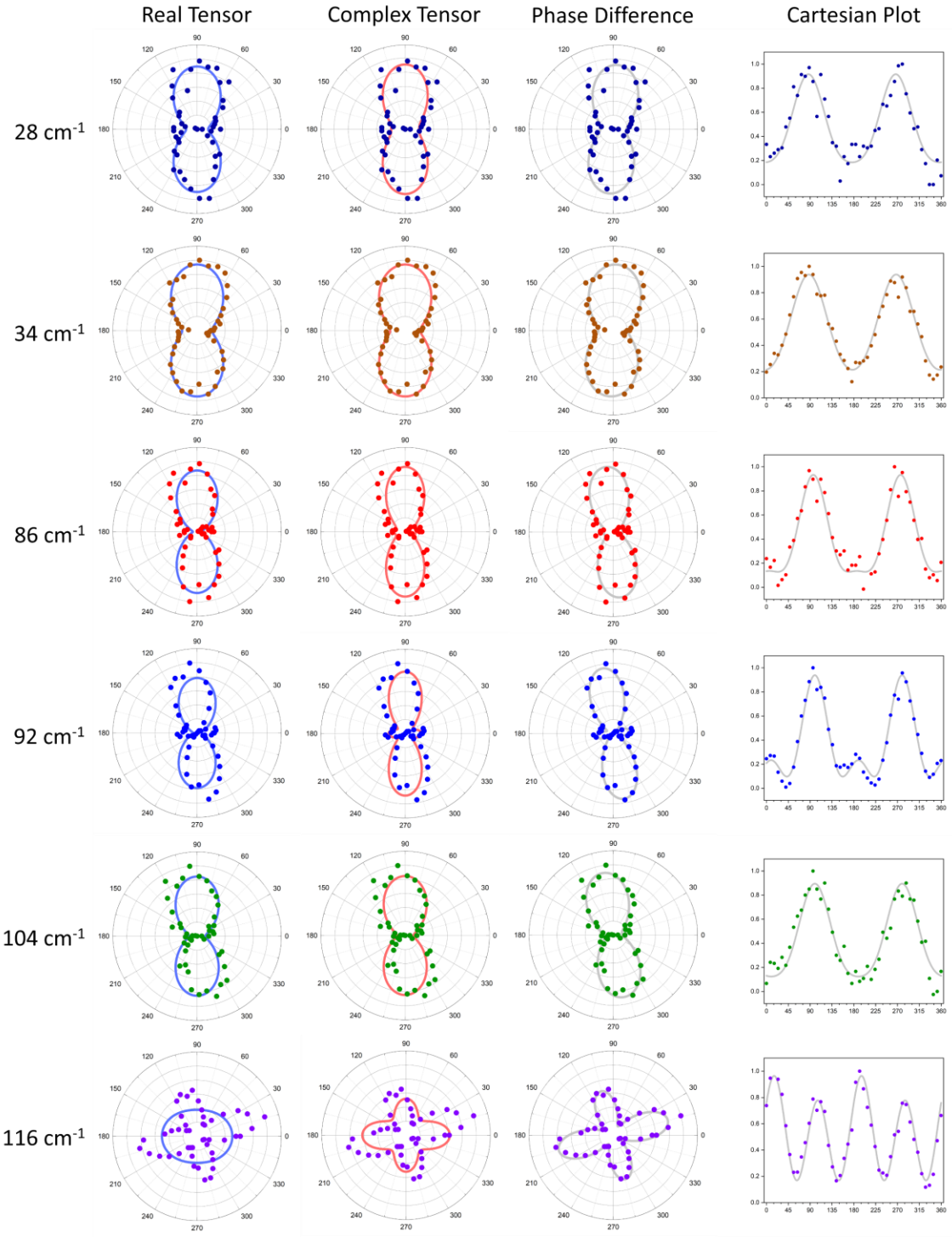

Supporting Figure S7(a). Experimental data (dots) for some Ag-like peaks in the parallel configuration (experiment in Figure 4 of the manuscript), fitted using real Raman tensor elements (eq. 2), complex Raman tensor elements (eq. 6), and considering the angular deviation (eq. 8). For clarity we have also added cartesian plots of the final fitting.

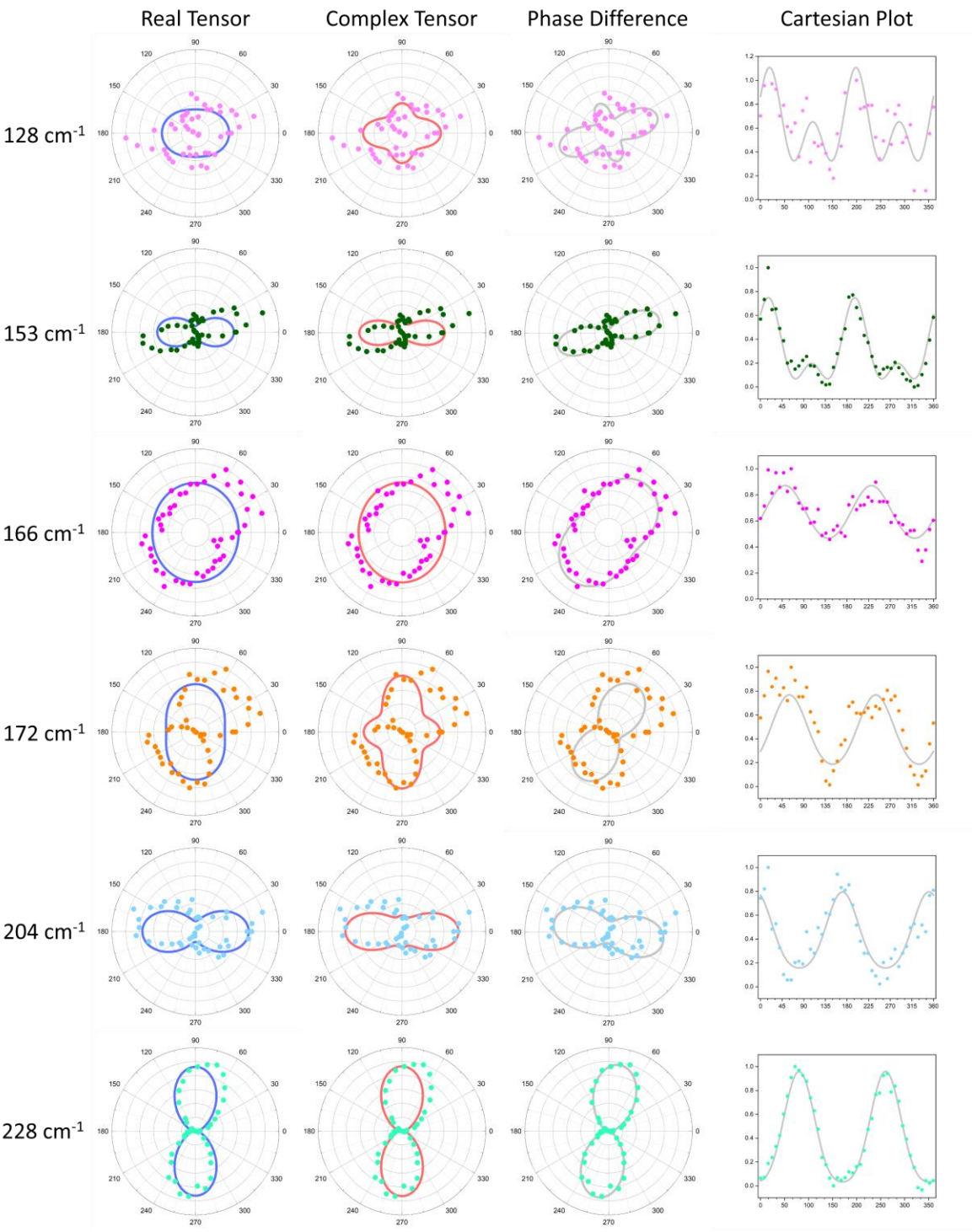

Supporting Figure S7(b). Experimental data (dots) for more Ag-like peaks in the parallel configuration (experiment in Figure 4 of the manuscript), fitted using real Raman tensor

elements (eq. 2), complex Raman tensor elements (eq. 6), and considering the angular deviation (eq. 8). For convenience and clarity we have also added cartesian plots of the final fitting.

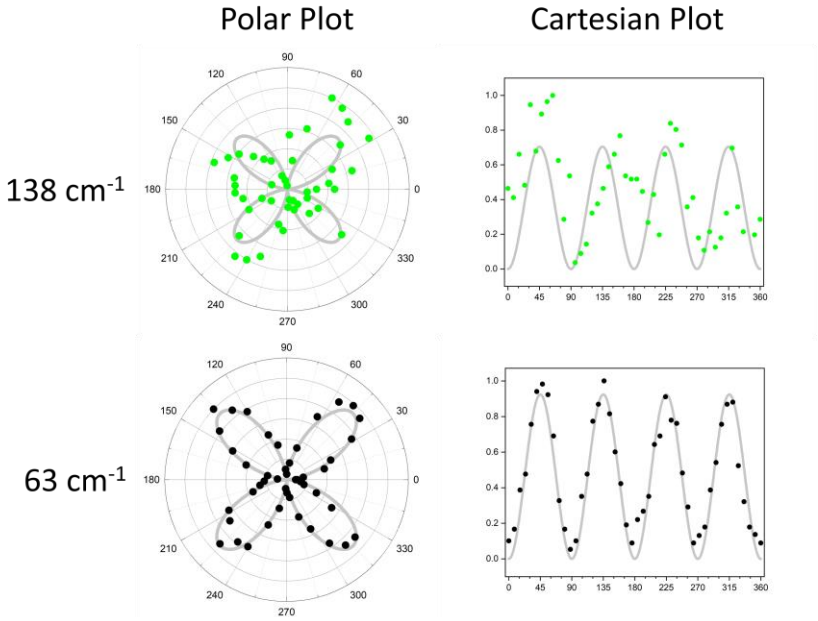

Supporting Figure S7(c). Experimental data (dots) for more B_{3g}-like peaks in the parallel configuration (experiment in Figure 4 of the manuscript), fitted using real Raman tensor elements (eq. 2).

S8. Fitting parameters for the Ag modes using equations (2) and (8), respectively.

Supporting Table S1:

Peak Position (cm^{-1})	Complex Tensor					Real Tensor		
	b	c	Φ (°)	φ (°)	c/b	b	c	c/b
28	3.57	7.95	-42.55	3.44	2.23	3.30	7.85	2.38
34	7.46	15.62	-36.49	2.63	2.09	7.46	15.62	2.09
63 (B_{3g})	-	-	-	-	-	-	-	-
86	4.129	10.84	81.54	-6.39	2.63	2.80	10.48	3.74
92	14.73	29.55	121.00	-9.69	2.01	7.45	26.97	3.62
104	3.86	10.37	-45.08	-9.68	2.69	3.77	10.09	2.68
116	32.97	29.60	127.43	-15.74	0.88	26.02	22.57	0.87
128	8.61	6.61	102.32	-18.68	0.77	6.98	5.86	0.84
138 (B_{3g})	-	-	-	-	-	-	-	-
153	15.98	8.19	-126.08	-16.20	0.51	13.69	5.51	0.40
166	14.64	20.00	-2.68	38.87	1.37	16.87	18.07	1.07
172	8.99	16.91	-21.29	29.45	1.88	12.52	15.97	1.28
204	8.41	3.74	-35.50	9.42	0.44	8.24	3.65	0.44
228	3.27	17.64	-4.06	9.65	5.39	3.93	17.3	4.40

S9. Raman Spectra for Parallel and Cross polarized Configurations along [001] and [010] Crystal Directions

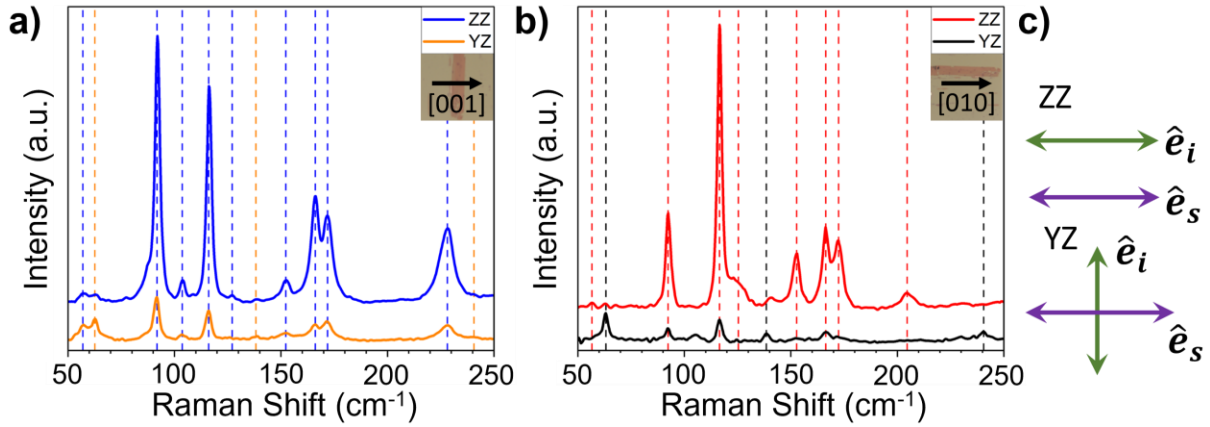

Supporting Figure S8. Summary of the polarized Raman spectra along the main in-plane crystallographic directions (a) [001] and (b) [010] for each polarization configuration. The color coded dashed lines indicate which peaks are characteristic to each polarization configuration. (c) A diagram showing scattering configurations for each sample orientation.

S10. Low Intensity Peaks Corresponding to Figure 6

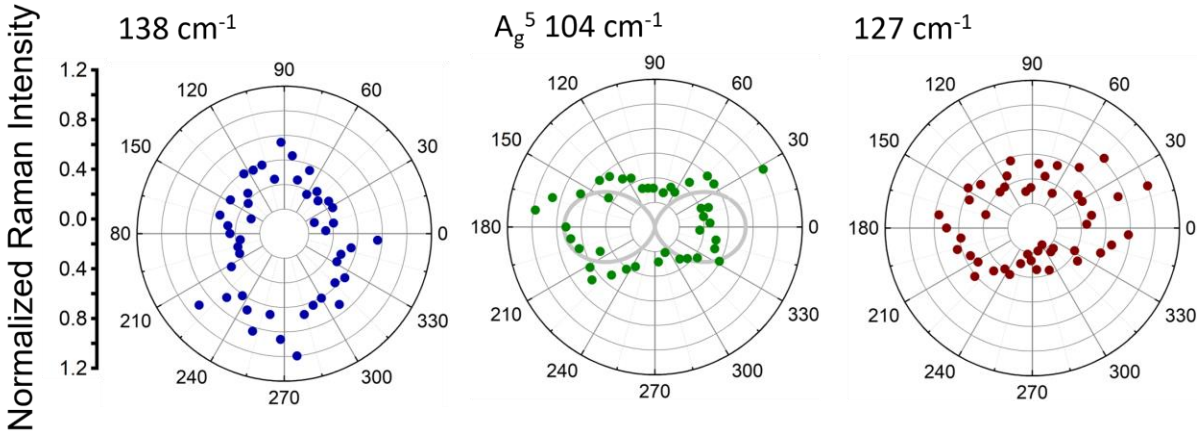

Supporting Figure S9. Additional polar plots corresponding to low intensity peaks observed for the experimental configuration used in Figure 6 of the manuscript.

S11. Stability of Raman Signal with Time

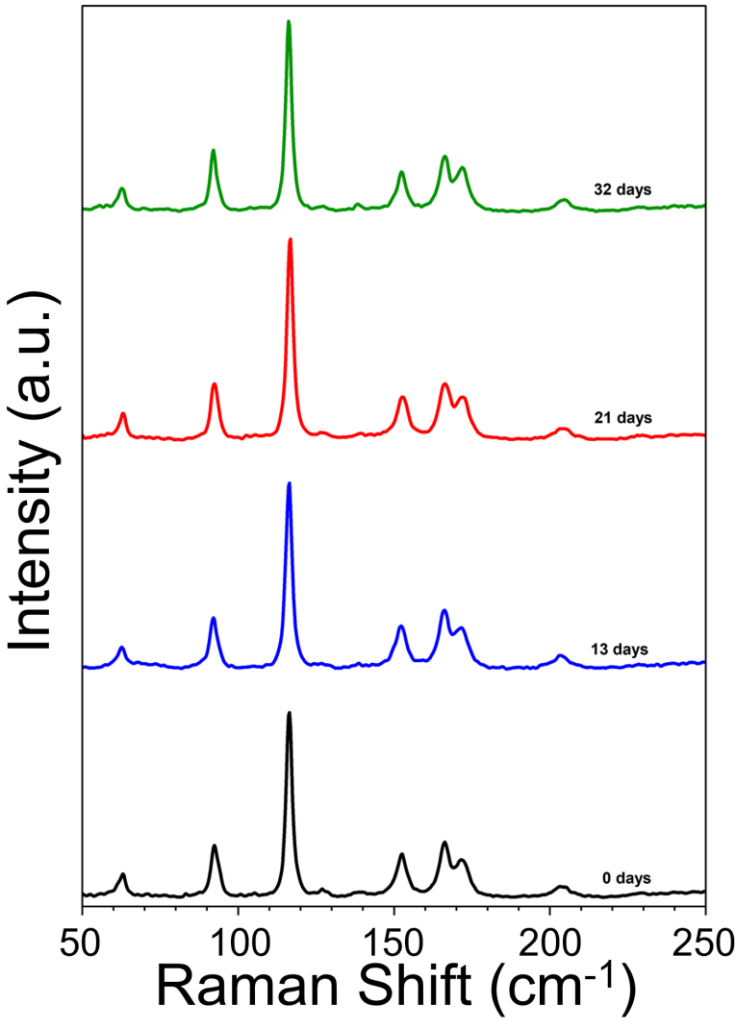

Supporting Figure S10. Stability test of the sample in air atmospheric conditions.

S12: Derivation of the light-polarization dependent equations for the different Raman mode intensities with <u>real tensor elements</u> in the Raman tensors:

We start considering the equation for the Raman intensity $I \propto |\hat{e}_i \cdot R \cdot \hat{e}_s|^2$

1.1- For the A_g modes in parallel polarization configuration:

$$I_{A_g}^{\parallel} \propto \left|(0 \quad cos\theta \quad sin\theta)\begin{pmatrix} a & 0 & 0 \\ 0 & b & 0 \\ 0 & 0 & c \end{pmatrix}\begin{pmatrix} 0 \\ cos\theta \\ sin\theta \end{pmatrix}\right|^2 \propto \left|(0 \quad b\,cos\theta \quad c\,sin\theta)\begin{pmatrix} 0 \\ cos\theta \\ sin\theta \end{pmatrix}\right|^2$$

$$I_{A_g}^{\parallel} \propto |b\,cos^2\theta + c\,sin^2\theta|^2$$ this is equation (2) in the main text

1.2- For the A_g modes in perpendicular polarization configuration:

$$I_{A_g}^{\perp} \propto \left|(0 \quad cos\theta \quad sin\theta)\begin{pmatrix} a & 0 & 0 \\ 0 & b & 0 \\ 0 & 0 & c \end{pmatrix}\begin{pmatrix} 0 \\ -sin\theta \\ cos\theta \end{pmatrix}\right|^2 \propto \left|(0 \quad b\,cos\theta \quad c\,sin\theta)\begin{pmatrix} 0 \\ -sin\theta \\ cos\theta \end{pmatrix}\right|^2$$

$$I_{A_g}^{\perp} \propto |-b\,cos\theta\,sin\theta + c\,cos\theta\,sin\theta|^2 \propto |(c-b)\,cos\theta\,sin\theta|^2$$

$$I_{A_g}^{\perp} \propto |(c-b)\,cos\theta\,sin\theta|^2$$ this is equation (3) in the main text

1.3- For the B_{3g} modes in parallel polarization configuration:

$$I_{B_{3g}}^{\parallel} \propto \left|(0 \quad cos\theta \quad sin\theta)\begin{pmatrix} 0 & 0 & 0 \\ 0 & 0 & f \\ 0 & f & 0 \end{pmatrix}\begin{pmatrix} 0 \\ cos\theta \\ sin\theta \end{pmatrix}\right|^2 \propto \left|(0 \quad f\,sin\theta \quad f\,cos\theta)\begin{pmatrix} 0 \\ cos\theta \\ sin\theta \end{pmatrix}\right|^2$$

$$I_{B_{3g}}^{\parallel} \propto |f\,cos\theta\,sin\theta + f\,cos\theta\,sin\theta|^2 \propto$$

$$I_{B_{3g}}^{\parallel} \propto |2f\,(cos\theta \cdot sin\theta)|^2$$ this is equation (4) in the main text

1.4- For the B_{3g} modes in perpendicular polarization configuration:

$$I_{B_{3g}}^{\perp} \propto \left|(0 \quad cos\theta \quad sin\theta)\begin{pmatrix}0 & 0 & 0\\ 0 & 0 & f\\ 0 & f & 0\end{pmatrix}\begin{pmatrix}0\\ -sin\theta\\ cos\theta\end{pmatrix}\right|^2 \propto \left|(0 \quad f\,sin\theta \quad f\,cos\theta)\begin{pmatrix}0\\ -sin\theta\\ cos\theta\end{pmatrix}\right|^2$$

$$I_{B_{3g}}^{\perp} \propto |f\,cos^2\theta - f\,sin^2\theta|^2 \propto$$

$$I_{B_{3g}}^{\perp} \propto |f\,cos(2\theta)|^2$$ this is equation (5) in the main text

1.5- For the B_{1g} modes in parallel polarization configuration:

$$I_{B_{1g}}^{\parallel} \propto \left|(0 \quad cos\theta \quad sin\theta)\begin{pmatrix}0 & d & 0\\ d & 0 & 0\\ 0 & 0 & 0\end{pmatrix}\begin{pmatrix}0\\ cos\theta\\ sin\theta\end{pmatrix}\right|^2 \propto \left|(d\,cos\theta \quad 0 \quad 0)\begin{pmatrix}0\\ cos\theta\\ sin\theta\end{pmatrix}\right|^2$$

$$I_{B_{1g}}^{\parallel} \propto |0|^2 \propto 0$$ Forbidden mode under this configuration

1.6- For the B_{1g} modes in perpendicular polarization configuration:

$$I_{B_{1g}}^{\perp} \propto \left|(0 \quad cos\theta \quad sin\theta)\begin{pmatrix}0 & d & 0\\ d & 0 & 0\\ 0 & 0 & 0\end{pmatrix}\begin{pmatrix}0\\ -sin\theta\\ cos\theta\end{pmatrix}\right|^2 \propto \left|(d\,cos\theta \quad 0 \quad 0)\begin{pmatrix}0\\ -sin\theta\\ cos\theta\end{pmatrix}\right|^2$$

$$I_{B_{1g}}^{\perp} \propto |0|^2 \propto 0$$ Forbidden mode under this configuration

1.7- For the B_{2g} modes in parallel polarization configuration:

$$I_{B_{2g}}^{\parallel} \propto \left|(0 \quad cos\theta \quad sin\theta)\begin{pmatrix}0 & 0 & e\\ 0 & 0 & 0\\ e & 0 & 0\end{pmatrix}\begin{pmatrix}0\\ cos\theta\\ sin\theta\end{pmatrix}\right|^2 \propto \left|(e\,sin\theta \quad 0 \quad 0)\begin{pmatrix}0\\ cos\theta\\ sin\theta\end{pmatrix}\right|^2$$

$$I_{B_{2g}}^{\parallel} \propto |0|^2 \propto 0$$ Forbidden mode under this configuration

1.8- For the B_{2g} modes in parallel polarization configuration:

$$I_{B_{2g}}^{\perp} \propto \left|(0 \quad cos\theta \quad sin\theta)\begin{pmatrix}0 & 0 & e\\ 0 & 0 & 0\\ e & 0 & 0\end{pmatrix}\begin{pmatrix}0\\ -sin\theta\\ cos\theta\end{pmatrix}\right|^2 \propto \left|(e\ sin\theta \quad 0 \quad 0)\begin{pmatrix}0\\ -sin\theta\\ cos\theta\end{pmatrix}\right|^2$$

$I_{B_{2g}}^{\perp} \propto |0|^2 \propto 0$ Forbidden mode under this configuration

1- Derivation of the light-polarization dependent equations for the different Raman mode intensities with <u>complex tensor elements</u> in the Raman tensors:

We use the above results for the intensity of each Raman mode but replace the real tensor elements with the complex tensor elements with the form:

$a \longrightarrow |a|e^{i\phi_a}$ $b \longrightarrow |b|e^{i\phi_b}$ $c \longrightarrow |c|e^{i\phi_c}$ $f \longrightarrow |f|e^{i\phi_f}$

2.1- For the A_g modes in <u>parallel</u> polarization configuration with complex tensor elements:

$$I_{A_g}^{\parallel} \propto |b\ cos^2\theta + c\ sin^2\theta|^2 \longrightarrow I_{A_g}^{\parallel} \propto \left||b|e^{i\phi_b}\ cos^2\theta + |c|e^{i\phi_c}\ sin^2\theta\right|^2$$

Multiplying by $e^{i\phi_c} \cdot e^{-i\phi_c}$ which is equal to 1:

$$I_{A_g}^{\parallel} \propto \left|e^{i\phi_c}(|b|e^{i(\phi_b-\phi_c)}\ cos^2\theta + |c|\ sin^2\theta)\right|^2$$

$$I_{A_g}^{\parallel} \propto \left|e^{i\phi_c}\right|^2 \cdot \left||b|e^{i(\phi_b-\phi_c)}\ cos^2\theta + |c|\ sin^2\theta\right|^2 = \left||b|e^{i\phi_{bc}}\ cos^2\theta + |c|\ sin^2\theta\right|^2$$

Where $\left|e^{i\phi_c}\right|^2 = 1$ and we called $\phi_{bc} = \phi_b - \phi_c$

$$I_{A_g}^{\parallel} \propto \left|(|b|e^{i\phi_{bc}}\ cos^2\theta + |c|\ sin^2\theta\right|^2$$

$$= |(|b|\ cos^2\theta\ cos\phi_{bc} + |c|\ sin^2\theta) + i\ \cdot (|b|\ cos^2\theta\ sin\phi_{bc})|^2$$

$$I_{A_g}^{\parallel} \propto (|b|\ cos^2\theta\ cos\phi_{bc} + |c|\ sin^2\theta)^2 + (|b|\ cos^2\theta\ sin\phi_{bc})^2$$

$$I_{A_g}^{\parallel} \propto [|c|sin^2\theta + |b|cos^2\theta\ cos\phi_{bc}]^2 + |b|^2cos^4\theta\ sin^2\phi_{bc}$$

And this is equation (6) in the main text.

2.2- For the A_g modes in <u>perpendicular</u> polarization configuration with complex tensor elements:

$$I_{A_g}^{\perp} \propto |(c-b)\, cos\theta\, sin\theta|^2 \longrightarrow I_{A_g}^{\perp} \propto \left|(|c|e^{i\phi_c} - |b|e^{i\phi_b})\, cos\theta\, sin\theta\right|^2$$

Multiplying by $e^{i\phi_c} \cdot e^{-i\phi_c}$ which is equal to 1:

$$I_{A_g}^{\perp} \propto \left|e^{i\phi_c}\,(|c| - |b|e^{i(\phi_b-\phi_c)})\, cos\theta\, sin\theta\right|^2$$

$$= \left|e^{i\phi_c}\right|^2 \left|\, |c| - |b|\, e^{i(\phi_b-\phi_c)}\right|^2 cos^2\theta\, sin^2\theta$$

$$= \left|\, |c| - |b|\, e^{i\phi_{bc}}\right|^2 cos^2\theta\, sin^2\theta$$

Where $\left|e^{i\phi_c}\right|^2 = 1$ and we called $\phi_{bc} = \phi_b - \phi_c$

And since $\left|\, |c| - |b|\, e^{i\phi_{bc}}\right|^2 = |(|c| - |b|\, cos\phi_{bc}) - i\,(|b|\, sin\phi_{bc})|^2$

$$= (|c| - |b|\, cos\phi_{bc})^2 + (|b|\, sin\phi_{bc})^2$$

Then:

$$I_{A_g}^{\perp} \propto [(|c| - |b|cos\phi_{bc})^2 + |b|^2 sin^2\phi_{bc}]\, sin^2\theta\, cos^2\theta$$

And this is equation (7) in the main text.

Notice that the B_{3g} modes intensities are not affected by the introduction of complex tensor elements since the complex exponential factors out and the square magnitude is always equal to 1.